Supporting information for "Seasonal variations of high time-resolved chemical compositions, sources and evolution for atmospheric submicron aerosols in the megacity Beijing"

Wei Hu, Min Hu*, Wei-Wei Hu, Jing Zheng, Chen Chen, Yusheng Wu, Song Guo

State Key Joint Laboratory of Environmental Simulation and Pollution Control, College of Environmental Sciences and Engineering, Peking University, Beijing 100871, China
*Corresponding author: minhu@pku.edu.cn

S1 Sampling site and measurements

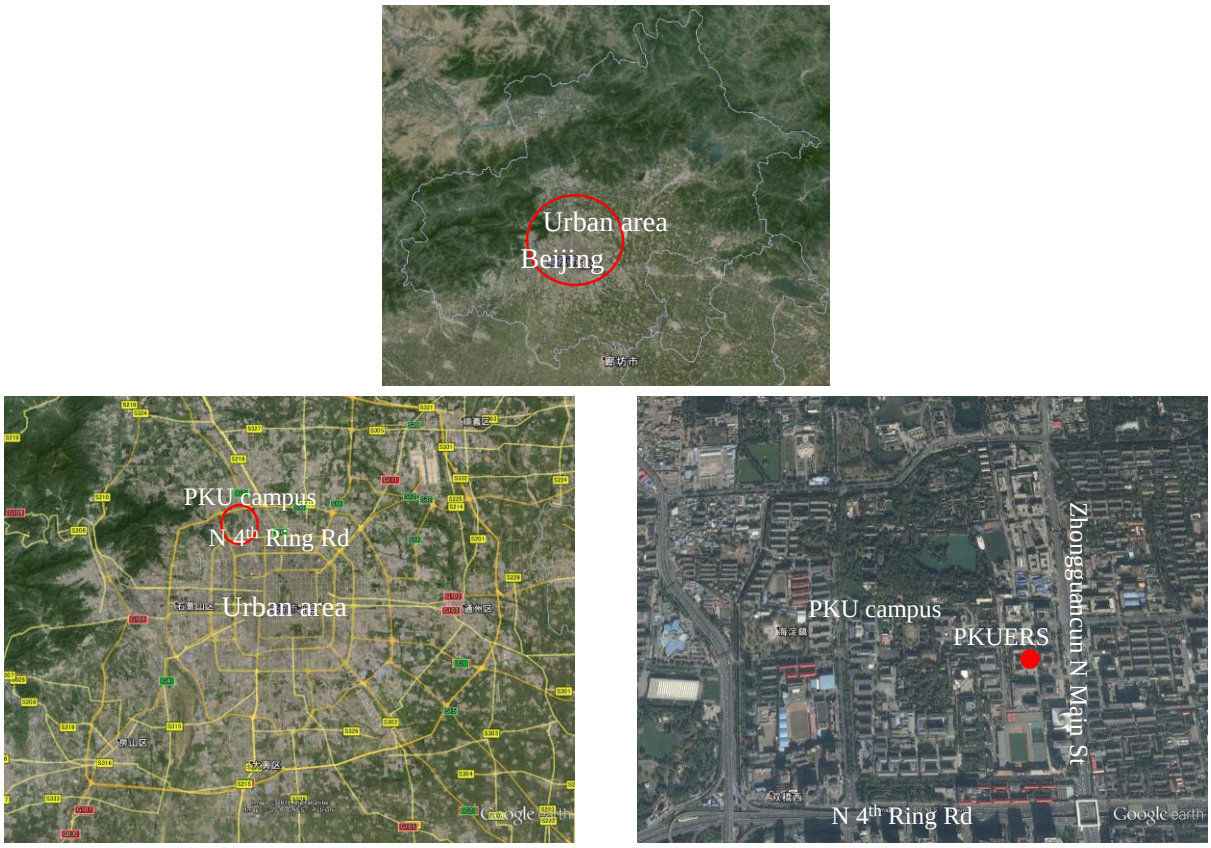

Figure S1. Location of observation site (PKUERS) and topographic map of Beijing.

Table S1 Measurement instrumentation for the campaigns.

Instrument	Parameters	Size	Time resolution	Manufacturer
HR-ToF-AMS	Mass concentrations size distributions of submicron non-refractory species	60~600 nm	4 min	Aerodyne Research Inc., USA
MAAP/Aethalometer	Particle absorption coefficient (BC)	2.5 μm	5 min	Thermo/Magee Scientific Co., USA
Semi-continuous EC/OC analyzer	Mass concentrations of OC and EC	2.5 μm	1 h	Sunset Lab Inc., USA
SMPS	Number concentrations of atmospheric particles	15~600 nm	5 min	TSI Inc., USA
TEOM 1400a, b	$PM_{2.5}$	2.5 μm	1 min	Thermo Scientific Co., USA
PTR-MS	Multiple volatile organic compounds (VOCs)		30 s	Ionicon Analytik, Austria
Gaseous pollutants	SO_2, NO_x, NO_y, CO, O_3		1 min	Ecotech Inc., USA
Meteorology	Wind speed and direction, temperature, relative humidity, atmospheric pressure		1 min	Met One Instruments Inc., USA

S2 Parameters of AMS instruments

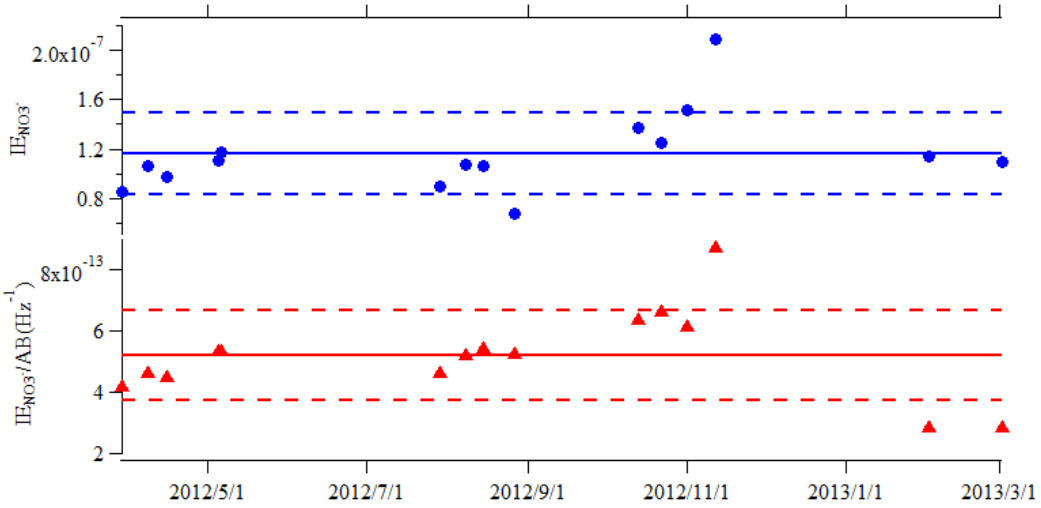

Figure S2. Ion efficiency (IE) and IE/air beam (AB) of AMS in this study. The dashed line is the standard deviation of the average IE/AB (solid line).

Table S3 Detection limits (V-mode) of main components of aerosol detected by AMS in this study. Units are μg m^{-3}. Detection limit of each species was determined by three times the standard deviations of detected signal of this species under particle-free condition.

Campaigns	OA	NO_3^-	SO_4^{2-}	NH_4^+	Cl^-
Spring	0.102	0.026	0.026	0.076	0.051
Summer	0.202	0.045	0.073	0.094	0.053
Autumn	0.337	0.019	0.017	0.068	0.025
Winter	0.072	0.016	0.022	0.043	0.014

S3 Comparison of results between AMS and other instruments, and ammonium balances

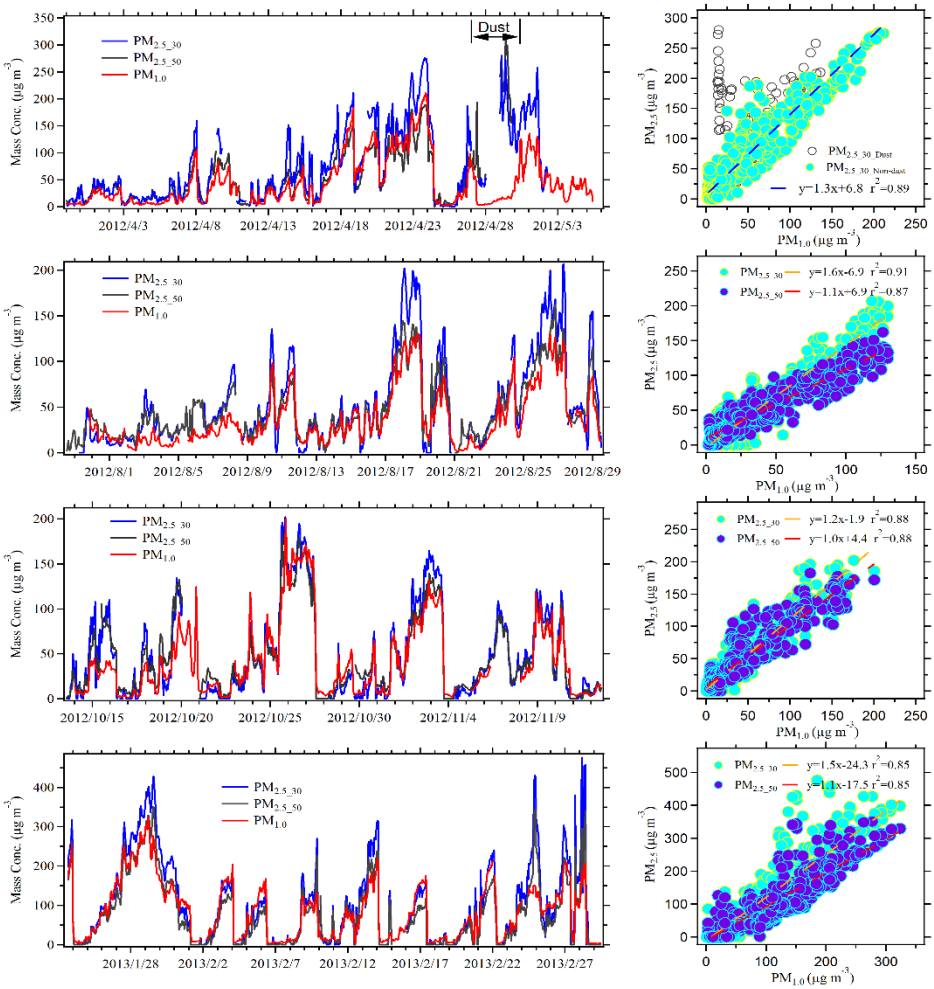

Figure S3. Time series and scatter plot of aerosol mass concentrations detected by AMS plus BC vs. TEOM during seasonal observations. The size cut off for BC is $PM_{2.5}$. The size cut of TEOM is $PM_{2.5}$, which should be the main reason that lower concentration in AMS+BC observed. $PM_{2.5\_30}$ and $PM_{2.5\_50}$ mean the concentrations of fine particles with dehumidification at 30°C and 50°C, respectively.

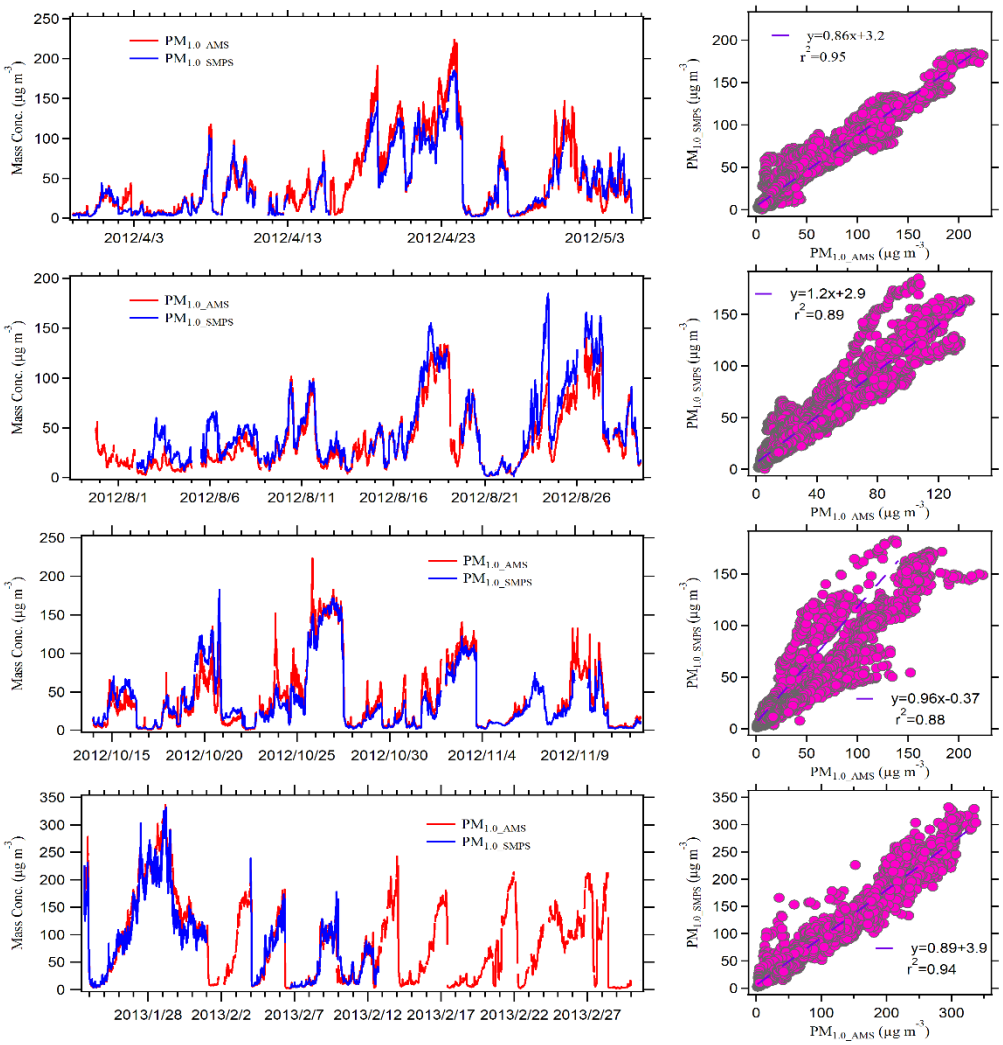

Figure S4. Time series and scatter plots of aerosol mass concentrations detected by AMS plus BC vs. SMPS during seasonal observations. The aerosol density based on chemical composition of aerosols was used to convert SMPS volume concentrations to be mass concentrations (Middlebrook et al., 2012).

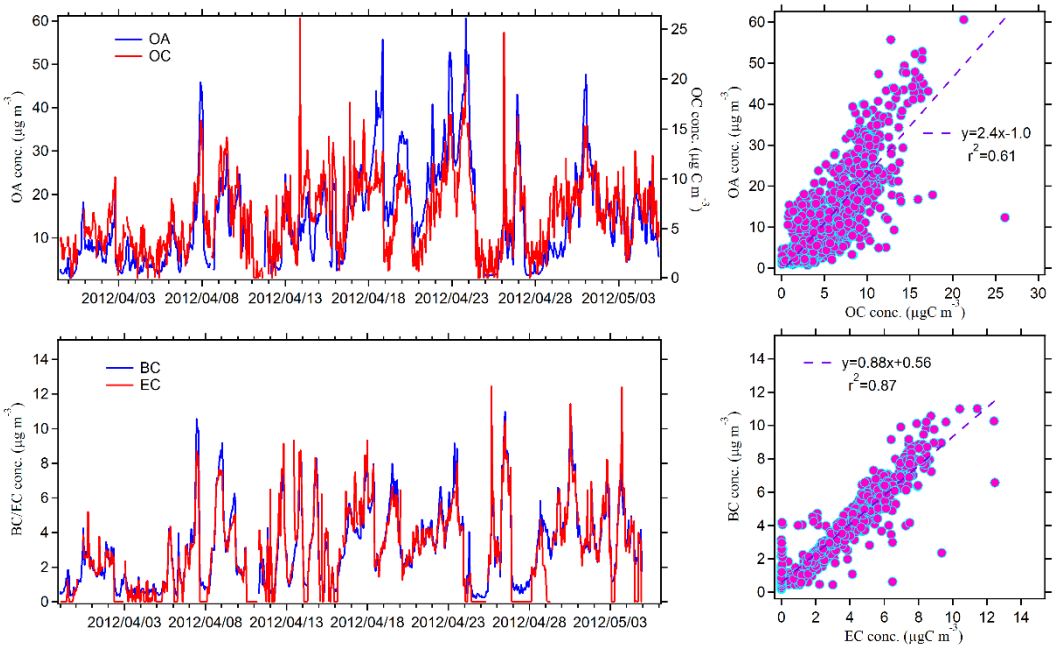

Figure S5. Time series and scatter plots of organic aerosol concentrations (OA) detected by AMS vs. organic carbon measured by a semi-continuous EC/OC analyzer, and BC vs. EC during the spring observation.

S4 Time series of meteorological parameters and main compositions in PM_1

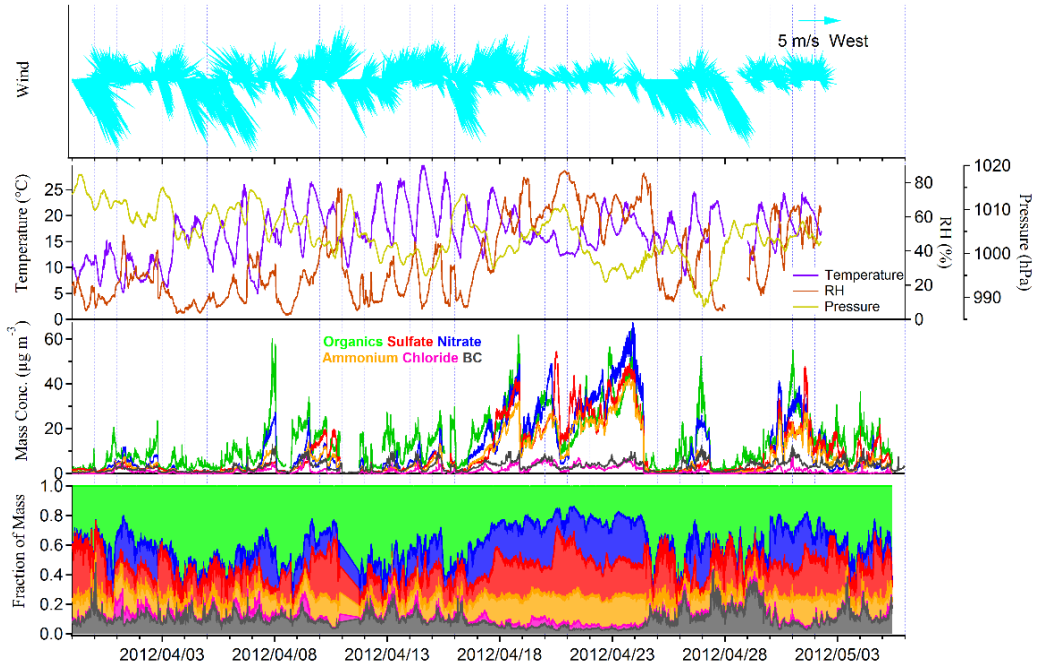

Figure S6. Time series of meteorological parameters (wind speed and direction, temperature, relative humidity (RH), and atmospheric pressure), and concentrations and fractions of main chemical compositions in submicron aerosols during the spring observation.

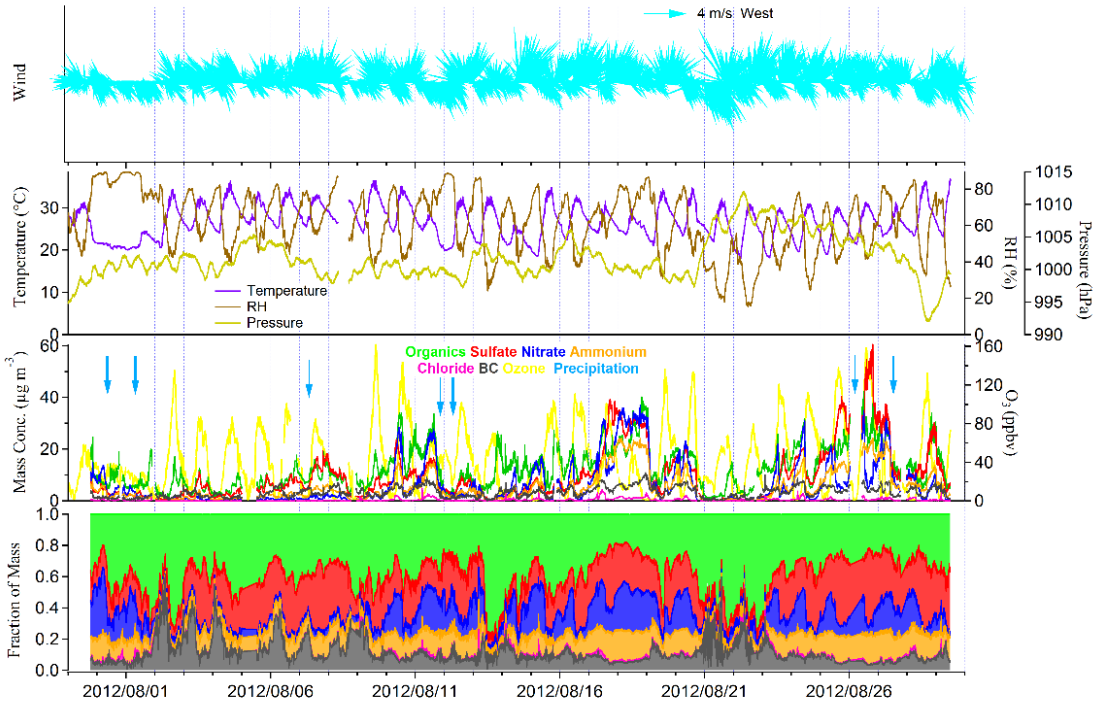

Figure S7. Time series of meteorological parameters (wind speed and direction, temperature, RH, and atmospheric pressure), and concentrations and fractions of main chemical compositions in submicron aerosols during the summer observation.

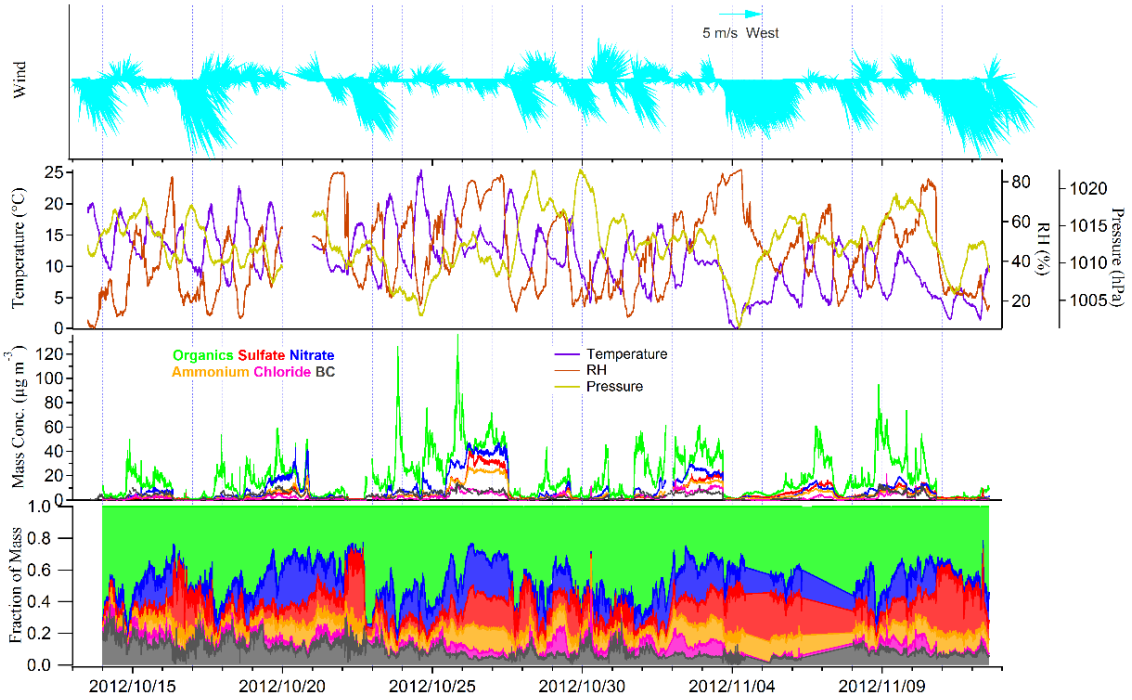

Figure S8. Time series of meteorological parameters (wind speed and direction, temperature, RH, and atmospheric pressure), and concentrations and fractions of main chemical compositions in submicron aerosols during the autumn observation.

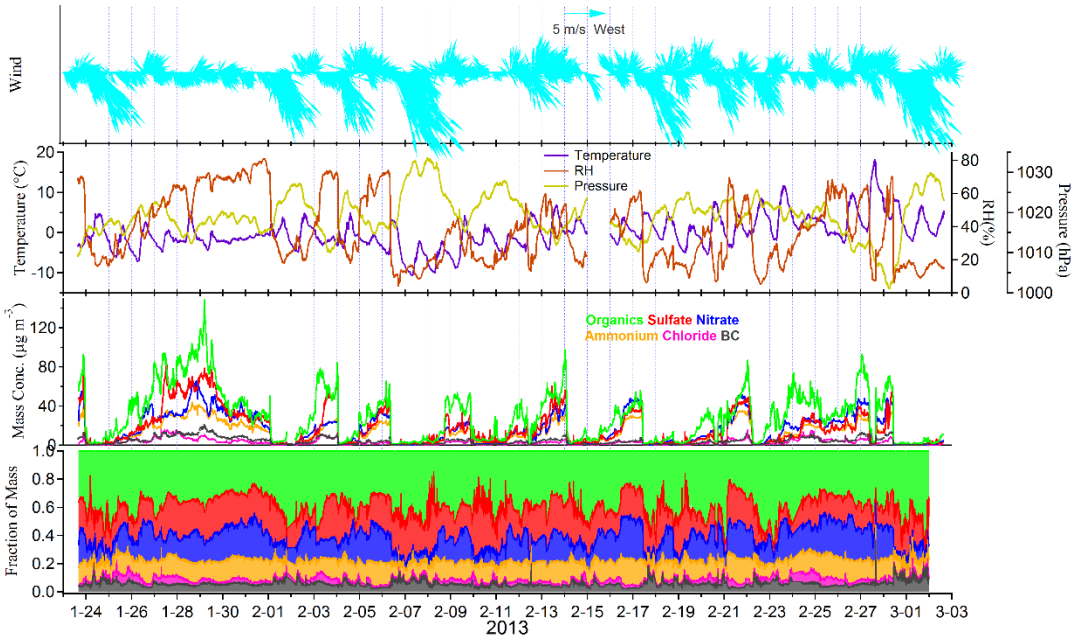

Figure S9. Time series of meteorological parameters (wind speed and direction, temperature, RH, and atmospheric pressure), and concentrations and fractions of main chemical compositions in submicron aerosols during the winter observation.

During four seasons, NOR ($\boldsymbol{n}$–NO_3^-/ ($\boldsymbol{n}$–NO_3^-+ $\boldsymbol{n}$–NO_2)) showed strong correlations with NH_4^+, indicating the main form of NO_3^- was NH_4NO_3. NH_4^+ also presented in the form of $(NH_4)_2SO_4$ and NH_4Cl. The predicted NH_4^+ was calculated assuming full neutralization of particulate anions of NO_3^-, SO_4^{2-}, and Cl^- in four seasons. The slopes of linear fitting of measured against predicted NH_4^+ in spring, summer, autumn and winter were 1.05, 1.02, 0.85, and 0.89, respectively. In autumn and winter, the relatively lower slopes implied that NH_4^+ was not enough to balance NO_3^-, SO_4^{2-} and Cl^-.

Field and emission studies have shown that a large fraction of KCl can exist in the fresh biomass burning plumes. As biomass burning plumes get aged, more S- and N- containing species (e.g., KNO_3 and K_2SO_4) in aerosol phase have been found (Li et al., 2003; Yokelson et al., 2009). It has also been reported that NaCl and NH_4Cl are important components in the aerosols directly emitted from biomass burning (Lewis et al., 2009; Levin et al., 2010). It was found that atmospheric aerosols were mostly acidic during heavy pollution episodes (Zhang et al, 2007; Sun et al, 2014.). During the heavy pollution periods in winter, SO_4^{2-} may exist in the form of NH_4HSO_4. Chloride existing in the form of KCl and NaCl in aerosol phase for coal combustion sources has been reported (McNallan et al., 1981; Doshi et al., 2009). Therefore,

NO_3^-, SO_4^{2-}, and Cl^- may exist as other forms in addition to ammonium due to the influences of intense autumn biomass burning and coal combustion in autumn and winter, respectively.

Table S4. Concentrations of main chemical components in PM_1 during seasonal observations in Beijing in recent years. Unit: μg m^{-3}.

Seasons	Periods	PM_1	OA	SO_4^{2-}	NO_3^-	NH_4^+	Cl^-	BC	References
Spring	10 Apr.-4 May. 2008	87.0	39.0						Zhang et al., 2013
	30 Mar.-7 May. 2012	**45.1**	**14.0**	**9.3**	**10.2**	**7.3**	**1.2**	**3.1**	**This study**
Summer	9-21 Jul. 2006	80.0	28.1	20.3	17.3	13.1	1.1		Sun et al., 2010
	24 Jul.-20 Sept. 2008	63.1	23.9	16.8	10.0	10.0	0.5	1.8	Huang et al., 2010
	5 Jun.-3 Jul. 2008	94.0	34.0	24.8	20.1	13.7	1.4		Zhang et al., 2013
	26 Jun.-28 Aug. 2011	50.0	20.0	9.0	12.4	8.0	0.5		Sun et al., 2012
	4 Aug.-14 Sept. 2011	84.3	26.4	22.0	16.8	13.7	1.0	4.4	Hu et al., 2016
	29 Jul.-29 Aug. 2012	**37.5**	**12.5**	**9.7**	**6.4**	**5.4**	**0.4**	**3.2**	**This study**
Autumn	4-18 Oct. 2008	51.0	24.0	8.1	12.0	6.2	0.7		Zhang et al., 2013
	1-30 Sept. 2012	40.9	17.1	6.4	8.1	5.1	0.5	3.7	Jiang et al., 2013
	13 Oct.-13 Nov. 2012	**41.3**	**18.2**	**5.5**	**7.9**	**4.5**	**2.0**	**3.2**	**This study**
Winter	4 Jan.-3 Feb. 2008	73.0	43.0	11.4	9.2	6.4	3.5		Zhang et al., 2013
	22 Nov.-22 Dec. 2010	69.5	34.5	8.7	6.8	7.7	5.8	6.0	Hu et al., 2016
	14 Dec. 2010-15 Jan. 2011		20.9						Liu et al., 2012
	21 Nov. 2011-20 Jan. 2012	66.8	34.4	9.4	10.7	8.7	3.3		Sun et al., 2013
	1-17 Jan. 2013	83.0	38.3	14.3	12.5	9.2	2.6	6.0	Sun et al., 2014
	1 Jan.-1 Feb. 2013	89.3	44.7	19.6	12.5	8.9	3.6		Zhang et al., 2014
	23 Jan.- 2 Mar. 2013	**81.7**	**29.7**	**17.4**	**16.2**	**11.7**	**2.8**	**3.9**	**This study**

S5 Concentration and mass spectra of OA factors

Table S5. Resolved fractions of OA during seasonal observations in Beijing in recent years. Unit: μg m^{-3}.

Seasons	Periods	LV-OOA[a]	SV-OOA[b]	OOA	LSOA	RSOA	HOA	CCOA	COA	BBOA	OOA/OA (%)	References
Spring	10 Apr.-4 May. 2008			23.0			16.0				59	Zhang et al., 2013
	30 Mar.-7 May. 2012	**4.3**	**4.6**				**1.4**		**3.7**		**63**	This study
Summer	9-21 Jul. 2006	12.6	4.5				11.0				61	Sun et al., 2010
	24 Jul.-20 Sept. 2008	8.1	5.7				4.3		5.8		58	Huang et al., 2010
	5 Jun.-3 Jul. 2008			20.0			14.0				59	Zhang et al., 2013
	26 Jun.-28 Aug. 2011			12.7			7.1				64	Sun et al., 2012
	4 Aug.-14 Sept. 2011	9.7	7.4				3.4		5.5		66	Hu et al., 2016
	29 Jul.-29 Aug. 2012	**3.3**	**5.3**				**1.4**		**2.5**		**69**	This study
Autumn	4-18 Oct. 2008			11.0			13.0				46	Zhang et al., 2013
	1-30 Sept. 2012			12.5			4.6				73	Jiang et al., 2013
	13 Oct.-13 Nov. 2012			**8.6**			**2.5**		**5.2**	**2.0**	**47**	This study
Winter	4 Jan.-3 Feb. 2008			10.0			33.0				23	Zhang et al., 2013
	22 Nov.-22 Dec. 2010	6.2	4.3				4.7	8.2	6.7	4.1	30	Hu et al., 2016
	14 Dec.2010-15 Jan. 2011			4.9			5.6		10.4		23	Liu et al., 2012
	21 Nov. 2011-20 Jan. 2012			10.7			5.8	11.4	6.5		31	Sun et al., 2013
	1-17 Jan. 2013		8.9		7.8	4.7	5.3	7.3	4.8		55	Sun et al., 2014
	1 Jan.-1 Feb. 2013	12.5	11.6				4.9	6.7	8.9		54	Zhang et al., 2014
	23 Jan.- 2 Mar. 2013	**9.8**	**5.0**				**5.5**	**5.1**	**4.3**		**50**	This study

Note: In Hu et al. (2016) and this study, [a] LV-OOA is defined as more-oxidized oxygenated OA (MO-OOA); [b] SV-OOA is defined as less-oxidized oxygenated OA (LO-OOA).

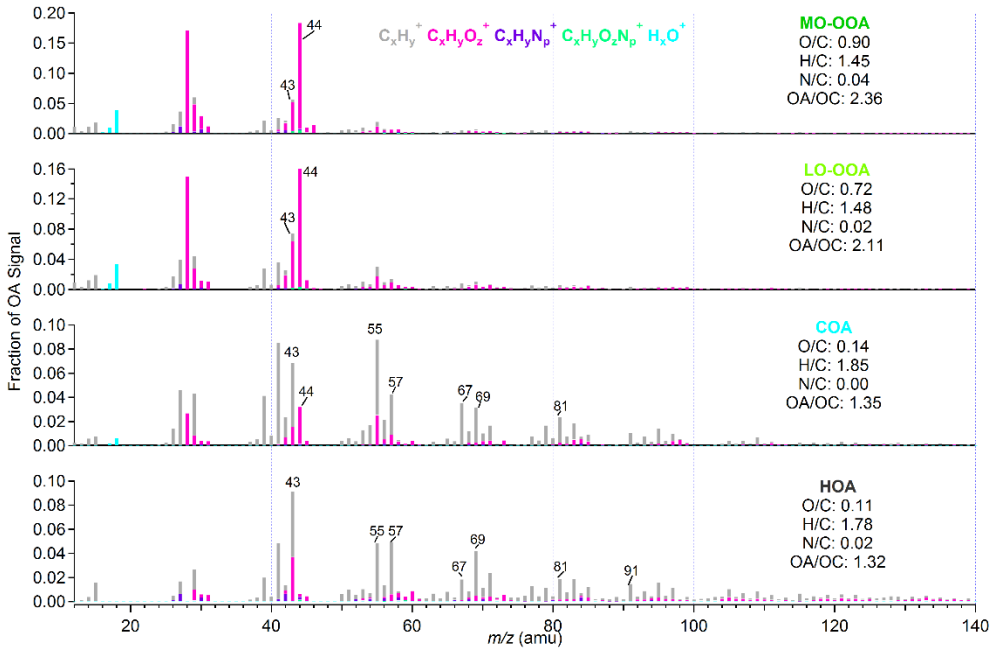

Figure S10. Unit mass spectra of OA factors resolved in the spring study: LV-OOA, SV-OOA, COA and HOA. The elemental ratios and OA/OC ratios of each component are also shown in the legends. The ion fragments are classified into five categories to identify the mass spectra characteristics: $C_xH_y^+$, $C_xH_yO_z^+$, $C_xH_yN_p^+$, $C_xH_yO_zN_p^+$ and H_xO^+ represent the reductive alkyl fragments, the oxygenated fragments of carboxylic acid and aldehyde, the nitrogen-containing alkyl fragments, the oxygenated organonitrogen fragment ions, and fragmented H_2O and carboxyl, respectively.

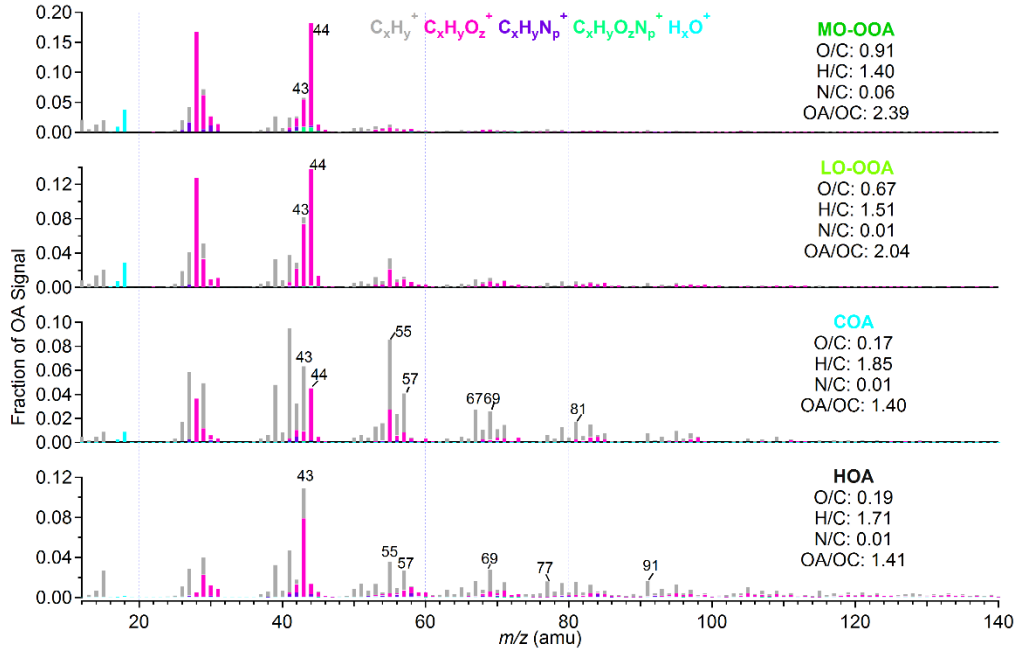

Figure S11. Unit mass spectra of OA factors resolved in the summer study: LV-OOA, SV-OOA, COA and HOA. The elemental ratios and OA/OC ratios of each component are also shown in the legends. The ion fragments are classified into five categories as described in Fig. S10.

The PMF analysis of the OA MS data set measured in autumn decomposed OOA factor into two, with similar MS characteristics (r= 0.976) and elemental ratios and OA/OC ratios (O/C: 0.85, 0.91; H/C: 1.24, 1.40; OA/OC: 2.24, 2.37), when selecting four factors as solution. When selecting five factors as solution, the split of OOA was similar, but more information on the OA sources (BBOA) can be provided. When selecting more than five factors, OOA decomposed into three or more factors. It was also found in other studies (e.g., Hayes et al., 2013). Therefore, the five factors, f_{Peak}=0 and seed=0 solution was chosen as the optimal solution for this PMF analysis, but two OOA factors were combined to total OOA. Finally, obtain four factors of OA were obtained, i.e., oxygenated OA (OOA), Cooking OA (COA), Hydrocarbon-like OA (HOA), and biomass burning OA(BBOA), as shown in Fig. S12. Due to the *m/z* 60 abundance in HOA was also high (~0.9%) in the autumn, the contribution of BBOA may be underestimated.

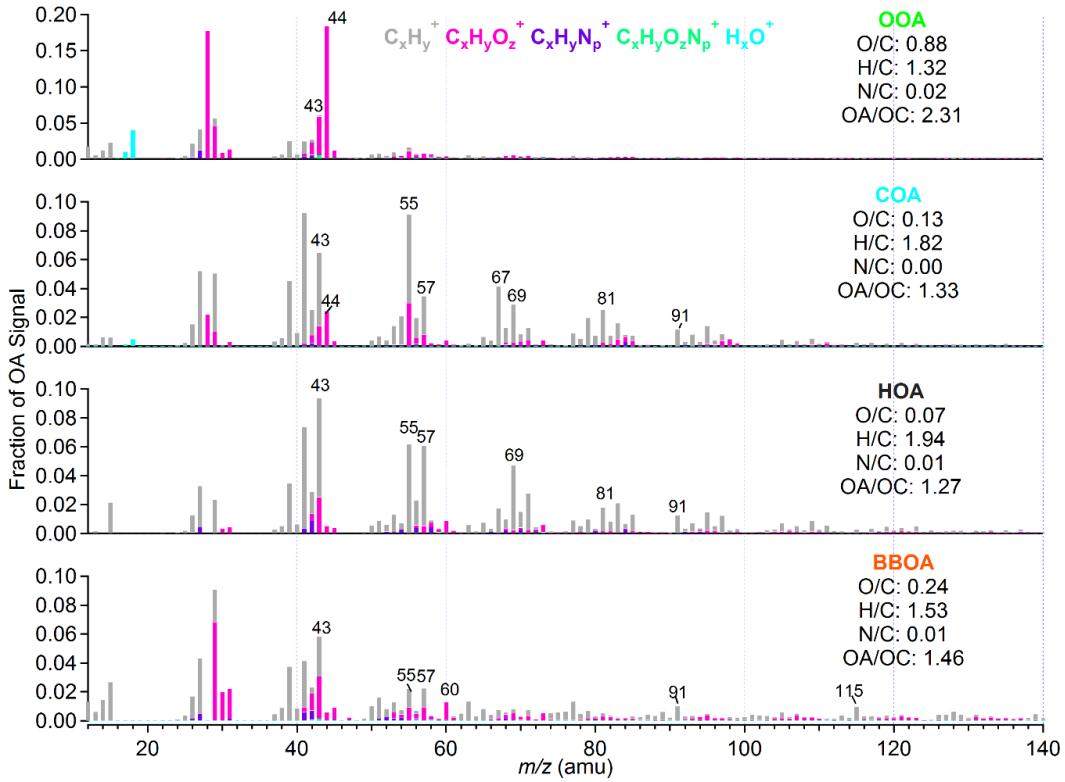

Figure S12. Unit mass spectra of OA factors resolved in the autumn study: OOA, COA, HOA, and BBOA. The elemental ratios and OA/OC ratios of each component are also shown in the legends. The ion fragments are classified into five categories as described in Fig. S10.

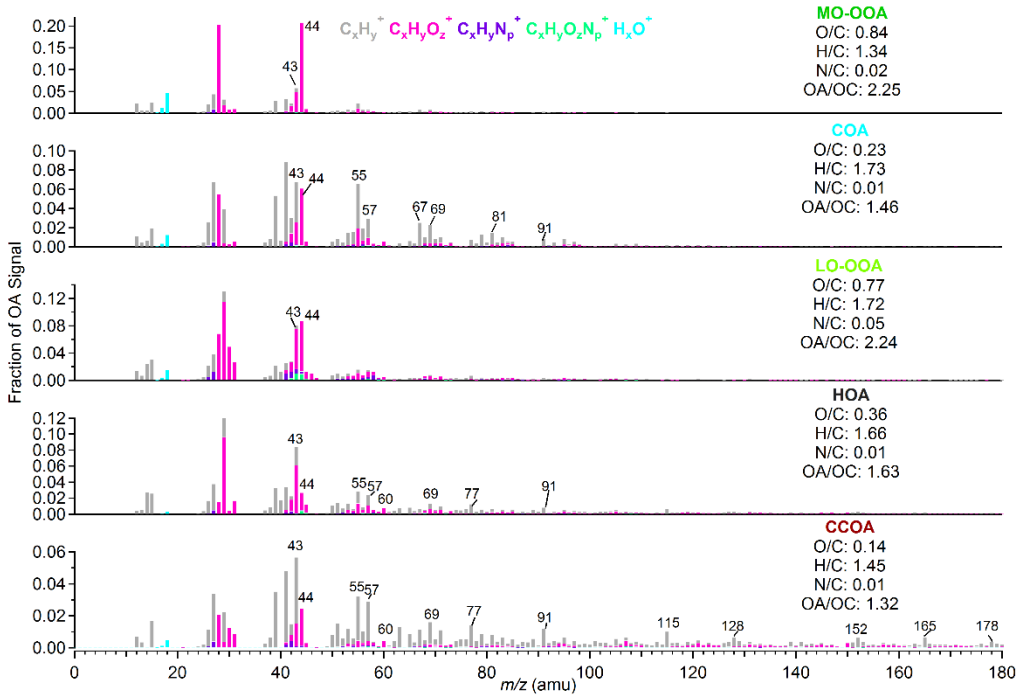

Figure S13. Unit mass spectra of OA factors resolved in the winter study: LV-OOA, LV-OOA, COA, HOA, and BBOA. The elemental ratios and OA/OC ratios of each component are also shown in the legends. The ion fragments are classified into five categories as described in Fig. S10.

S6 Time series of OA fractions

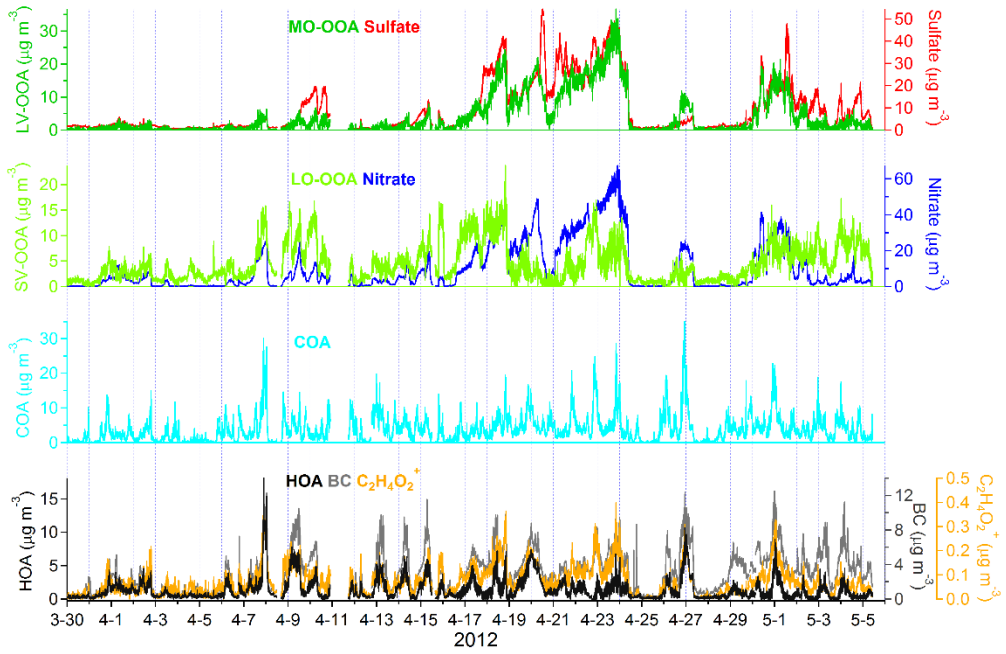

Figure S14. Time series of OA fractions and external tracers (sulfate, nitrate, BC, and $C_2H_4O_2^+$) during the spring observation.

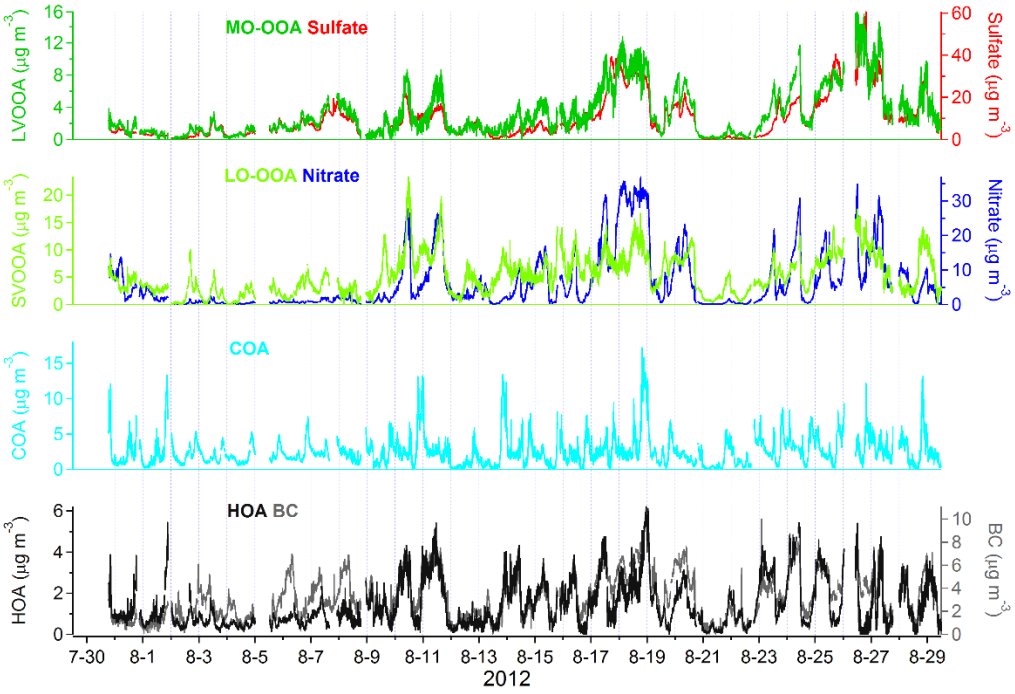

Figure S15. Time series of OA fractions and external tracers (sulfate, nitrate, and BC) during the summer observation.

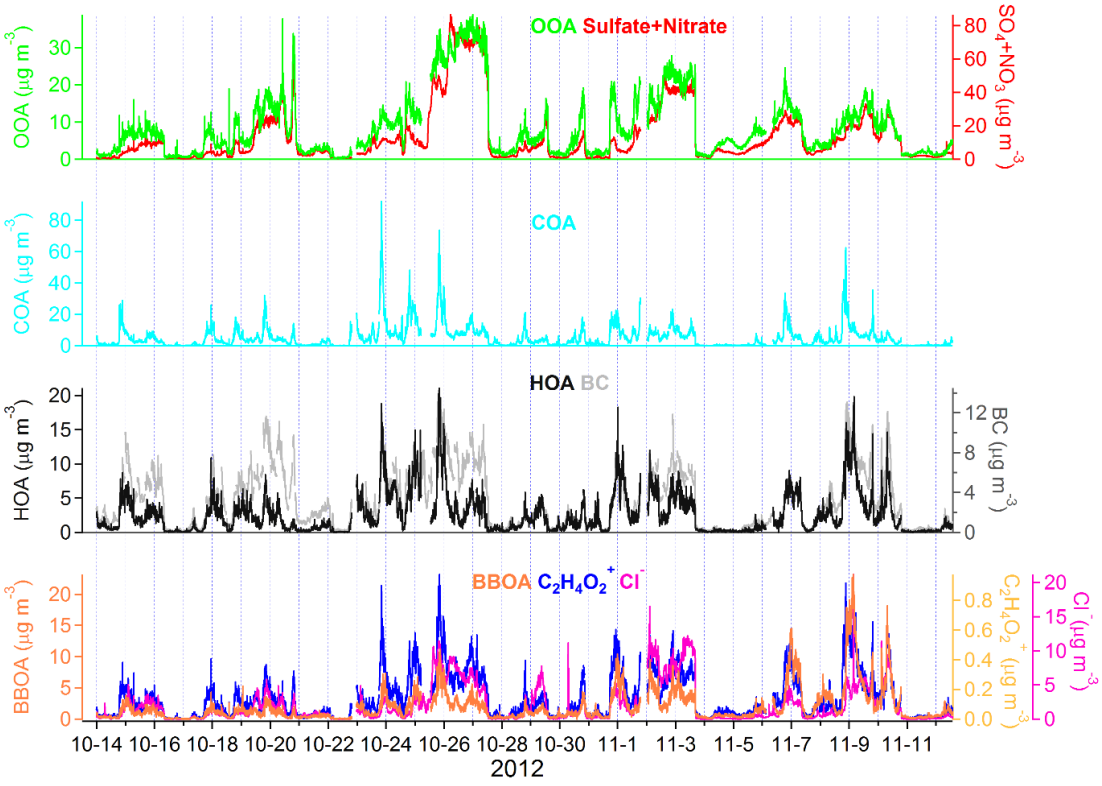

Figure S16. Time series of OA fractions and external tracers (sulfate+nitrate, BC, chloride and $C_2H_4O_2^+$) during the autumn observation.

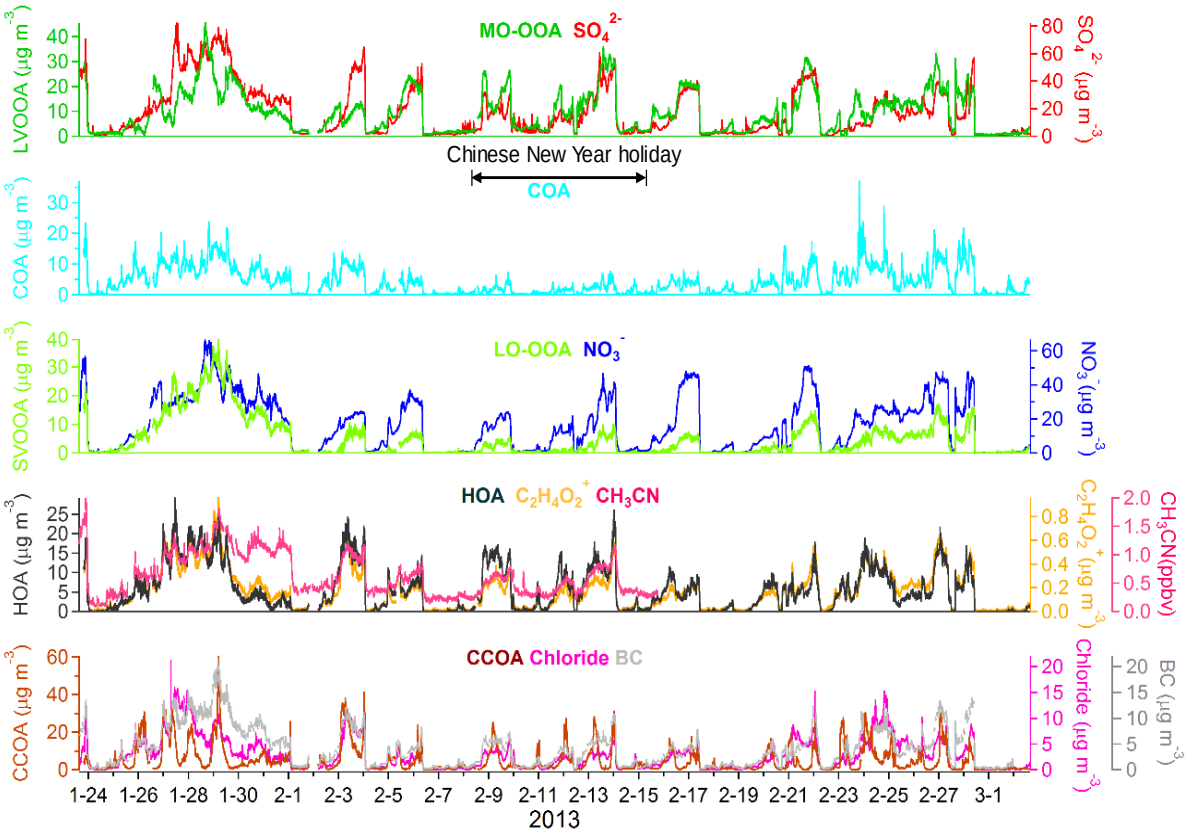

Figure S17. Time series of OA fractions and external tracers (sulfate, nitrate, $C_2H_4O_2^+$, acetonitrile, chloride and BC) during the winter observation.

S7 Elemental compositions of OA

The diurnal variations of element ratios (O/C, H/C) and OA/OC ratios were obvious during the seasonal observations in Beijing (Fig. S18-S21). The diurnal patterns of O/C and OA/OC ratios in the spring, summer and autumn were similar: during the daytime, the oxidation state of OA gradually increased due to the effect of photochemical reactions; the O/C and OA/OC ratios were peaked at about 16:00 in the afternoon, indicating that secondary formation is an important factor affecting the properties of OA. As the products of photochemical reactions, SOA gradually accumulated in the daytime, making an important contribution to OA. In the morning, the O/C and OA/OC ratios declined slightly at 7:00-8:00, which may be affected by reductive OA emitted from vehicles during the rush hour. They showed two valleys at noon (12:00-13:00) and in the evening (19:00-20:00), reflecting the impacts of cooking emissions during meal time (Huang et al., 2010). In the autumn, the oxidation state of OA (O/C and OA/OC ratio) maintained at a low level after the valley at 20:00,

mainly caused by the biomass emissions at night. While in the summer, the O/C and OA/OC ratios rose after 20:00, indicating the aqueous oxidation processes may play a significant role under high humidity conditions at nighttime (Ervens et al., 2011). In the winter, the diurnal patterns of O/C and OA/OC ratios were close to those in other seasons, but the impacts of vehicular and cooking emissions were less significant than in other seasons; the oxidation state of OA kept to decrease after 20:00, which is mainly influenced by primary emissions (e.g., coal combustion and biomass burning) at night. Hydrogen mainly comes from the alkyl fragments. Along with oxidation of OA, alkyl functional groups are gradually substituted by oxygenated ones, the proportion of hydrogen in OA is gradually reduced. Therefore, the diurnal variations of H/C ratios always trended oppositely with those of O/C and OA/OC ratios.

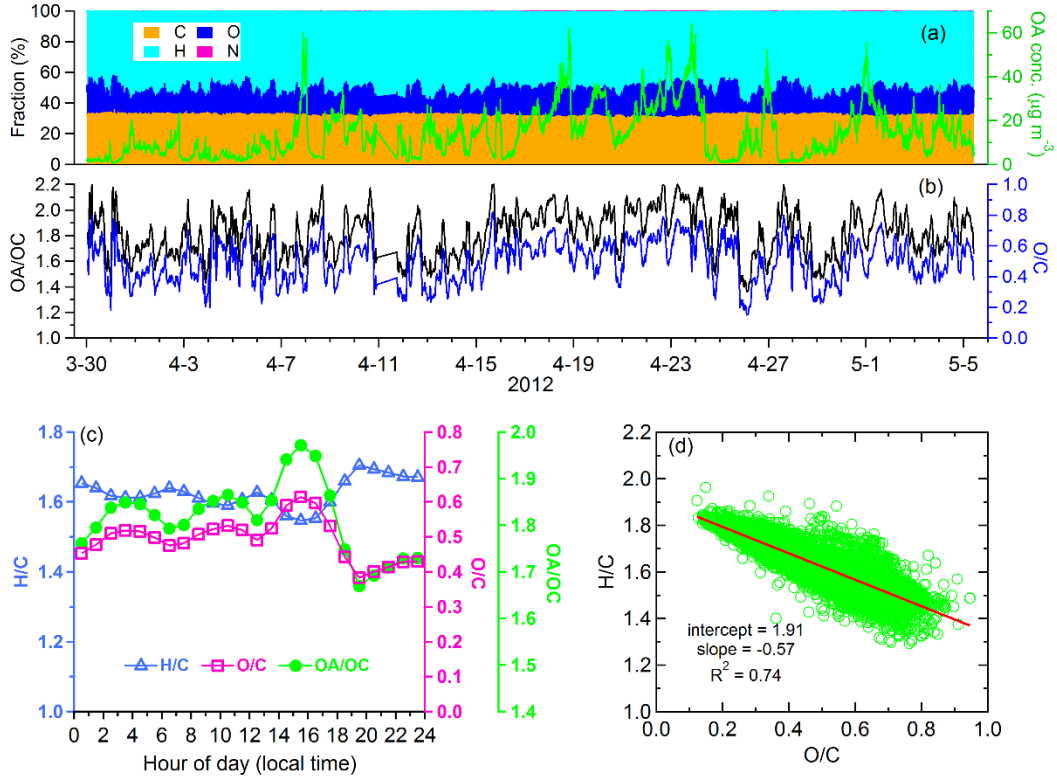

Figure S18. Time series of (a) elemental fractions and (b) OA/OC and O/C ratios in OA; (c) Diurnal patterns of OA/OC, H/C and O/C ratios; (d) van Krevelen diagram of OA during the spring observation.

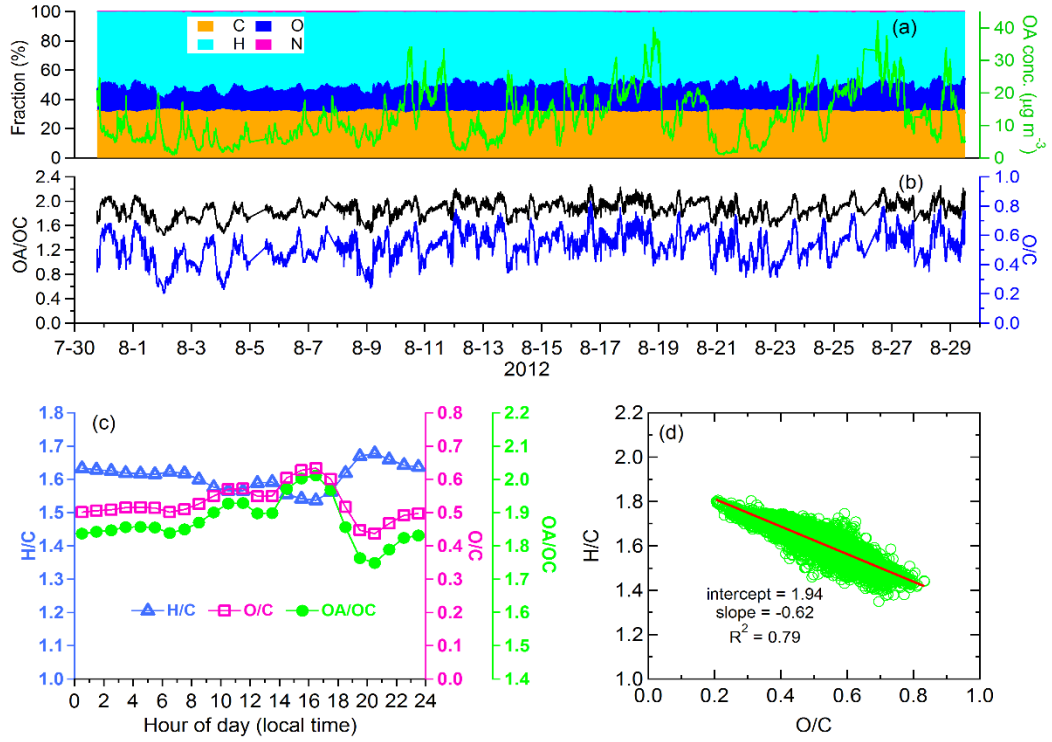

Figure S19. Time series of (a) elemental fractions and (b) OA/OC and O/C ratios in OA; (c) Diurnal patterns of OA/OC, H/C and O/C ratios; (d) van Krevelen diagram of OA during the summer observation.

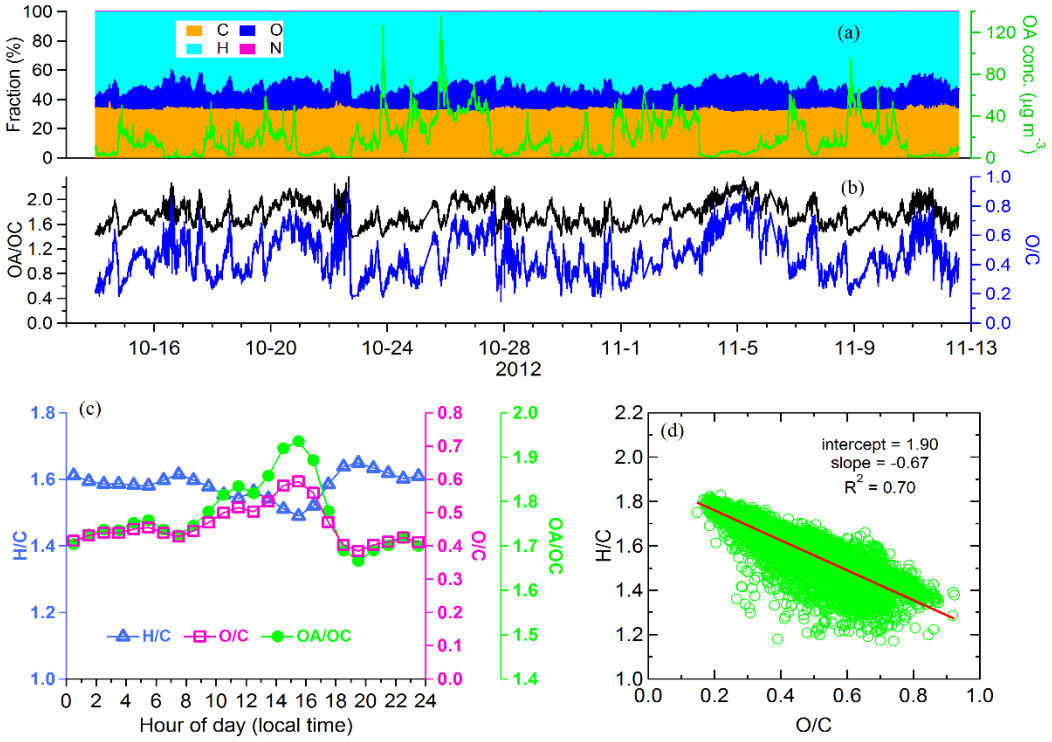

Figure S20. Time series of (a) elemental fractions and (b) OA/OC and O/C ratios in OA; (c) Diurnal patterns of OA/OC, H/C and O/C ratios; (d) van Krevelen diagram of OA during the autumn observation.

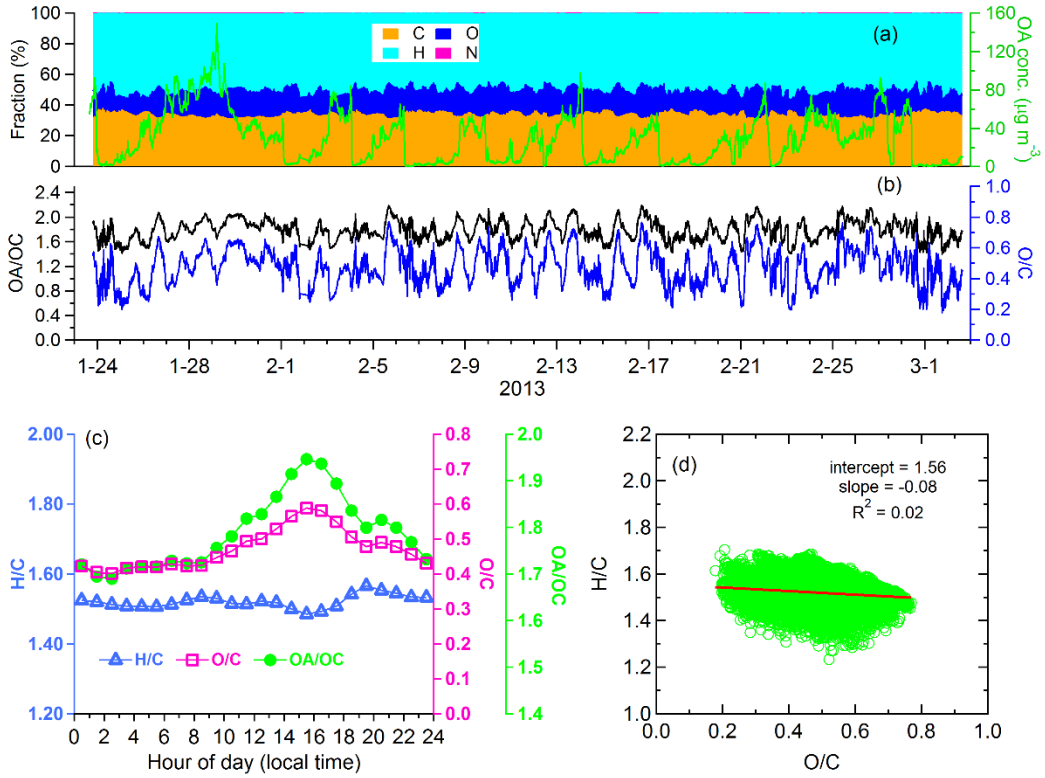

Figure S21. Time series of (a) elemental fractions and (b) OA/OC and O/C ratios in OA; (c) Diurnal patterns of OA/OC, H/C and O/C ratios; (d) van Krevelen diagram of OA during the winter observation.

S8 Correlation matrix of gaseous pollutants and particulate chemical compositions

Table S6 Correlation matrix of gaseous pollutants and particulate chemical compositions in submicron aerosols during the spring campaign.

	CO	NO_x	SO_2	O_3	O_x	SO_4^{2-}	NO_3^-	NH_4^+	Cl^-	BC	$C_2H_4O_2^+$	LV-OOA	SV-OOA	COA	HOA
CO	1.000														
NO_x	.475	1.000													
SO_2	.755	.301	1.000												
O_3	-.376	-.679	-.051	1.000											
O_x	.219	.029	.485	.561	1.000										
SO_4^{2-}	.758	.189	.531	-.205	.186	1.000									
NO_3^-	.773	.361	.550	-.314	.258	.871	1.000								
NH_4^+	.798	.300	.577	-.282	.231	.953	.973	1.000							
Cl^-	.764	.480	.598	-.461	.094	.667	.755	.771	1.000						
BC	.615	.826	.513	-.532	.275	.454	.635	.580	.676	1.000					
$C_2H_4O_2^+$	.591	.580	.448	-.396	.342	.556	.716	.670	.674	.822	1.000				
MO-OOA	.766	.320	.492	-.299	.206	.908	.971	.973	.727	.574	.661	1.000			
LO-OOA	.268	.194	.437	.015	.504	.392	.457	.445	.380	.544	.677	.362	1.000		
COA	.420	.647	.222	-.423	.251	.255	.393	.340	.374	.656	.745	.357	.250	1.000	
HOA	.436	.740	.347	-.560	.075	.168	.376	.307	.614	.804	.717	.300	.371	.578	1.000

Table S7 Correlation matrix of gaseous pollutants and particulate chemical compositions in submicron aerosols during the summer campaign.

	CO	NO_x	SO_2	O_3	O_x	SO_4^{2-}	NO_3^-	NH_4^+	Cl^-	BC	$C_2H_4O_2^+$	LV-OOA	SV-OOA	COA	HOA
CO	1.000														
NO_x	.456	1.000													
SO_2	.354	-.027	1.000												
O_3	-.041	-.541	.382	1.000											
O_x	.124	-.310	.431	.957	1.000										
SO_4^{2-}	.620	.099	.644	.261	.351	1.000									
NO_3^-	.718	.334	.321	-.123	-.007	.657	1.000								
NH_4^+	.720	.213	.555	.098	.205	.932	.882	1.000							
Cl^-	.625	.441	.186	-.252	-.145	.463	.795	.668	1.000						
BC	.773	.672	.270	-.232	-.030	.604	.740	.715	.727	1.000					
$C_2H_4O_2^+$	.697	.469	.327	.030	.227	.667	.702	.737	.619	.773	1.000				
MO-OOA	.663	.260	.529	.129	.252	.912	.813	.946	.651	.756	.745	1.000			
LO-OOA	.601	.196	.320	.382	.543	.642	.626	.682	.449	.613	.816	.691	1.000		
COA	.428	.449	.100	-.135	.035	.266	.238	.274	.217	.415	.646	.222	.310	1.000	
HOA	.558	.741	.036	-.404	-.203	.255	.626	.443	.710	.787	.705	.498	.469	.423	1.000

Table S8 Correlation matrix of gaseous pollutants and particulate chemical compositions in submicron aerosols during the autumn campaign.

	CO	NO_x	SO_2	O_3	O_x	SO_4^{2-}	NO_3^-	NH_4^+	Cl^-	BC	$C_2H_4O_2^+$	OOA	COA	HOA	BBOA
CO	1.000														
NO_x	.639	1.000													
SO_2	.694	.379	1.000												
O_3	-.511	-.694	-.319	1.000											
O_x	.517	.371	.566	-.044	1.000										
SO_4^{2-}	.789	.334	.458	-.332	.335	1.000									
NO_3^-	.827	.447	.521	-.373	.541	.943	1.000								
NH_4^+	.838	.423	.522	-.379	.462	.976	.987	1.000							
Cl^-	.855	.532	.618	-.477	.367	.745	.753	.804	1.000						
BC	.833	.851	.516	-.636	.465	.595	.691	.676	.732	1.000					
$C_2H_4O_2^+$	.761	.741	.431	-.536	.383	.560	.631	.629	.743	.864	1.000				
OOA	.834	.526	.510	-.419	.567	.901	.969	.957	.775	.746	.733	1.000			
COA	.499	.671	.223	-.398	.430	.272	.393	.351	.391	.638	.798	.502	1.000		
HOA	.590	.812	.286	-.567	.236	.302	.383	.376	.578	.812	.908	.493	.785	1.000	
BBOA	.606	.573	.407	-.439	.156	.352	.359	.383	.613	.728	.827	.433	.487	.816	1.000

Table S9 Correlation matrix of gaseous pollutants and particulate chemical compositions in submicron aerosols during the winter campaign.

	CO	NO_x	SO_2	CH_3CN	O_3	O_x	SO_4^{2-}	NO_3^-	NH_4^+	Cl^-	BC	$C_2H_4O_2^+$	LV-OOA	COA	SV-OOA	HOA	CCOA
CO	1.000																
NO_x	.933	1.000															
SO_2	.682	.702	1.000														
CH_3CN	.914	.895	.669	1.000													
O_3	-.763	-.757	-.701	-.712	1.000												
O_x	.692	.755	.561	.723	-.404	1.000											
SO_4^{2-}	.852	.826	.635	.852	-.635	.727	1.000										
NO_3^-	.813	.790	.627	.844	-.651	.804	.898	1.000									
NH_4^+	.854	.824	.652	.861	-.668	.777	.971	.971	1.000								
Cl^-	.790	.795	.572	.733	-.623	.555	.801	.666	.778	1.000							
BC	.922	.917	.646	.899	-.696	.749	.911	.850	.902	.874	1.000						
$C_2H_4O_2^+$	.833	.826	.555	.807	-.634	.644	.847	.774	.835	.889	.945	1.000					
MO-OOA	.562	.504	.493	.593	-.461	.702	.783	.872	.855	.463	.644	.603	1.000				
COA	.806	.879	.539	.808	-.655	.690	.765	.753	.778	.797	.859	.830	.480	1.000			
LO-OOA	.842	.880	.590	.844	-.556	.833	.887	.857	.877	.747	.902	.819	.627	.817	1.000		
HOA	.699	.658	.509	.666	-.587	.514	.797	.695	.781	.839	.839	.916	.666	.670	.636	1.000	
CCOA	.618	.561	.317	.520	-.515	.151	.432	.318	.387	.648	.635	.751	.086	.527	.408	.667	1.000

Table S10 Uncentered coefficients between mass spectra of COA factors during the seasonal campaigns in Beijing and the average from previous studies.

	Spring	**Summer**	**Autumn**	**Winter**	**Average**
Spring	1.000				
Summer	0.988	1.000			
Autumn	0.925	0.888	1.000		
Winter	0.947	0.977	0.835	1.000	
Average	0.996	0.990	0.910	0.954	1.000

References

Doshi, V., Vuthaluru, H. B., Korbee, R., and Kiel, J. H. A.: Development of a modeling approach to predict ash formation during co-firing of coal and biomass, Fuel Process Technol, 90, 1148-1156, doi: 10.1016/j.fuproc.2009.05.019, 2009.

Ervens, B., Turpin, B., and Weber, R.: Secondary organic aerosol formation in cloud droplets and aqueous particles (aqSOA): a review of laboratory, field and model studies, Atmos. Chem. Phys., 11, 11069-11102, 2011.

Hayes, P. L., Ortega, A. M., Cubison, M. J., Froyd, K. D., Zhao, Y., Cliff, S. S., Hu, W. W., Toohey, D. W., Flynn, J. H., Lefer, B. L., Grossberg, N., Alvarez, S., Rappenglück, B., Taylor, J. W., Allan, J. D., Holloway, J. S., Gilman, J. B., Kuster, W. C., de Gouw, J. A., Massoli, P., Zhang, X., Liu, J., Weber, R. J., Corrigan, A. L., Russell, L. M., Isaacman, G., Worton, D. R., Kreisberg, N. M., Goldstein, A. H., Thalman, R., Waxman, E. M., Volkamer, R., Lin, Y. H., Surratt, J. D., Kleindienst, T. E., Offenberg, J. H., Dusanter, S., Griffith, S., Stevens, P. S., Brioude, J., Angevine, W. M., and Jimenez, J. L.: Organic aerosol composition and sources in Pasadena, California, during the 2010 CalNex campaign, J. Geophys. Res. Atmos., 118, 9233-9257, 2013.

Hu, W. W., Hu, M., Hu, W., Jimenez, J. L., Yuan, B., Chen, W., Wang, M., Wu, Y., Chen, C., Wang, Z., Peng, J., Yang, K., Zeng, L., and Shao, M.: Chemical composition, sources and aging process of sub-micron aerosols in Beijing: contrast between summer and winter, J. Geophys. Res.-Atmos., 121, 1955–1977, doi: 10.1002/2015JD024020, 2016.

Huang, X. F., He, L. Y., Hu, M., Canagaratna, M. R., Sun, Y., Zhang, Q., Zhu, T., Xue, L., Zeng, L. W., Liu, X. G., Zhang, Y. H., Jayne, J. T., Ng, N. L., and Worsnop, D. R.: Highly time-resolved chemical characterization of atmospheric submicron particles during 2008 Beijing Olympic Games using an Aerodyne High-Resolution Aerosol Mass Spectrometer, Atmos. Chem. Phys., 10, 8933-8945, 2010.

Jiang, Q., Sun, Y., Wang, Z., Yin, Y.: Real-time online measurements of the inorganic and organic composition of haze fine particles with an Aerosol Chemical Speciation Monitor (ACSM). Chin. Sci. Bull., 58, 3818-3828, 2013.

Levin, E. J. T., McMeeking, G. R., Carrico, C. M., Mack, L. E., Kreidenweis, S. M., Wold, C. E., Moosmüller, H., Arnott, W. P., Hao, W. M., Collett, J. L., and Malm, W. C.: Biomass burning smoke aerosol properties measured during Fire Laboratory at Missoula Experiments (FLAME), J. Geophys. Res. Atmos., 115, doi: 10.1029/2009jd013601, 2010.

Lewis, K. A., Arnott, W. P., Moosmuller, H., Chakrabarty, R. K., Carrico, C. M., Kreidenweis, S. M., Day, D. E., Malm, W. C., Laskin, A., Jimenez, J. L., Ulbrich, I. M., Huffman, J. A., Onasch, T. B., Trimborn, A., Liu, L., and Mishchenko, M. I.: Reduction in biomass burning aerosol light absorption upon humidification: roles of inorganically-induced hygroscopicity, particle collapse, and photoacoustic heat and mass transfer, Atmos. Chem. Phys., 9, 8949-8966, 2009.

Li, J., Pósfai, M., Hobbs, P. V., and Buseck, P. R.: Individual aerosol particles from biomass burning in southern Africa: 2, Compositions and aging of inorganic particles, J. Geophys. Res. Atmos., 108, D13, 8484, 2003.

Liu, Q., Sun, Y., Hu, B., Liu, Z., Akio, S., and Wang, Y.: In situ measurement of PM1 organic

aerosol in Beijing winter using a high-resolution aerosol mass spectrometer, Chin. Sci. Bull., 57, 819-826, 2011.

McNallan, M. J., Yurek, G. J., and Elliott, J. F.: The formation of inorganic particulates by homogeneous nucleation in gases produced by the combustion of coal, Combustion and Flame, 42, 45-60, doi:10.1016/0010-2180(81)90141-3, 1981.

Middlebrook, A. M., Bahreini, R., Jimenez, J. L., and Canagaratna, M. R.: Evaluation of Composition-Dependent Collection Efficiencies for the Aerodyne Aerosol Mass Spectrometer using Field Data, Aerosol Sci. Technol., 46, 258-271, doi:10.1080/02786826.2011.620041, 2012.

Sun, J., Zhang, Q., Canagaratna, M. R., Zhang, Y., Ng, N. L., Sun, Y., Jayne, J. T., Zhang, X., Zhang, X., and Worsnop, D. R.: Highly time- and size-resolved characterization of submicron aerosol particles in Beijing using an Aerodyne Aerosol Mass Spectrometer, Atmos. Environ., 44, 131-140, 2010.

Sun, Y., Wang, Z., Dong, H., Yang, T., Li, J., Pan, X., Chen, P., and Jayne, J. T.: Characterization of summer organic and inorganic aerosols in Beijing, China with an Aerosol Chemical Speciation Monitor, Atmos. Environ., 51, 250-259, 2012.

Sun, Y., Jiang, Q., Wang, Z., Fu, P., Li, J., Yang, T., and Yin, Y.: Investigation of the sources and evolution processes of severe haze pollution in Beijing in January 2013, J. Geophys. Res. Atmos., 119, 4380-4398, 2014.

Sun, Y. L., Wang, Z. F., Fu, P. Q., Yang, T., Jiang, Q., Dong, H. B., Li, J., and Jia, J. J.: Aerosol composition, sources and processes during wintertime in Beijing, China, Atmos. Chem. Phys., 13, 4577-4592, 2013.

Yokelson, R. J., Crounse, J. D., DeCarlo, P. F., Karl, T., Urbanski, S., Atlas, E., Campos, T., Shinozuka, Y., Kapustin, V., Clarke, A. D., Weinheimer, A., Knapp, D. J., Montzka, D. D., Holloway, J., Weibring, P., Flocke, F., Zheng, W., Toohey, D., Wennberg, P. O., Wiedinmyer, C., Mauldin, L., Fried, A., Richter, D., Walega, J., Jimenez, J. L., Adachi, K., Buseck, P. R., Hall, S. R., and Shetter, R.: Emissions from biomass burning in the Yucatan, Atmos. Chem. Phys., 9, 5785-5812, 2009.

Zhang, J. K., Sun, Y., Liu, Z. R., Ji, D. S., Hu, B., Liu, Q., and Wang, Y. S.: Characterization of submicron aerosols during a month of serious pollution in Beijing, 2013, Atmos. Chem. Phys., 14, 2887-2903, 2014.

Zhang, Q., Jimenez, J. L., Canagaratna, M. R., Allan, J. D., Coe, H., Ulbrich, I., Alfarra, M. R., Takami, A., Middlebrook, A. M., Sun, Y. L., Dzepina, K., Dunlea, E., Docherty, K., DeCarlo, P. F., Salcedo, D., Onasch, T., Jayne, J. T., Miyoshi, T., Shimono, A., Hatakeyama, S., Takegawa, N., Kondo, Y., Schneider, J., Drewnick, F., Borrmann, S., Weimer, S., Demerjian, K., Williams, P., Bower, K., Bahreini, R., Cottrell, L., Griffin, R. J., Rautiainen, J., Sun, J. Y., Zhang, Y. M., and Worsnop, D. R.: Ubiquity and dominance of oxygenated species in organic aerosols in anthropogenically-influenced Northern Hemisphere midlatitudes, Geophys. Res. Lett., 34, 2007.

Zhang, Y., Sun, J., Zhang, X., Shen, X., Wang, T., and Qin, M.: Seasonal characterization of components and size distributions for submicron aerosols in Beijing, Sci. China Earth Sci., 56, 890-900, 2013.